The influence of plasma waves on the dispersion of surface plasmons : experimental evidence

M. Abraham, A. Tadjeddine

J. Physique **48** (1987) 267-275 FÉVRIER **1987**, PAGE 267

Classification
Physics Abstracts
07.60H — 78.65

The influence of plasma waves on the dispersion of surface plasmons : experimental evidence

M. Abraham and A. Tadjeddine (*)

TH Ilmenau, DDR, 6300 Ilmenau, PSF 327, G.D.R.
(*) L.E.I du C.N.R.S. 1, place A. Briand, 92195 Meudon Ppl. Cedex, France

(*Reçu le 3 juin 1986, révisé le 6 octobre, accepté le 10 octobre 1986*)

Résumé. — Des mesures d'excitation des plasmons de surface par réflexion totale atténuée ont été réalisées dans un large domaine spectral, entre 1,9 et 5 eV sur des substrats d'aluminium recouverts de films minces continus d'argent. Les résultats sont discutés sur la base du modèle hydrodynamique des électrons libres aussi bien dans le film que dans le substrat, ce qui conduit à introduire des conditions aux limites supplémentaires. L'interprétation des résultats expérimentaux (relation de dispersion et courbes de réflectivité) nécessite la prise en compte des ondes longitudinales de plasma. Une nouvelle branche de la courbe de dispersion des plasmons de surface est mise en évidence entre 4,2 et 4,6 eV. Elle est attribuée au couplage entre l'onde de plasma et les modes de surface localisés dans la queue de la densité de charge aux interfaces.

Abstract. — Surface plasmon excitation by attenuated total reflection in Otto geometry has been carried out in a wide spectral range between 1.9 and 5 eV. Samples were Al-films covered by thin (5 nm) continuous Ag-layers. Results were discussed in the framework of a hydrodynamic model of the conduction electrons both in the film and in the substrate using additional boundary conditions. The calculated and measured dispersion relation and reflectivity curves show that longitudinal plasma waves have to be taken into account. A new branch of the surface plamon dispersion is found experimentally between 4.2 and 4.6 eV. It is attributed to coupled plasma wave-surface plasmon modes localized in the tail of the electronic charge density at the interfaces.

1. Introduction.

Optical excitation of surface plasmons (SP) is now established as a valuable tool for the investigation of the metal-dielectric interface and of very thin coatings deposited on free electron like metals (see e.g. the reviews in [1]). SP's are collective oscillations of conduction electrons confined at the interface between an active medium and a dielectric. Their localization makes SP's very sensitive to the properties of the interface, where they can be excited optically by attenuated total reflection (ATR) and detected by reflectometry or ellipsometry. In electrochemistry this technique has been successfully applied to *in situ* studies of the metal-electrolyte interface [2-4]. The set-up used by Tadjeddine in this field in previous work [13] is based on the principle of ATR by focused light proposed by Kretschmann [5]. Most of these studies have been done on Ag which is both a « good » electrode (no chemical reactions in a wide potential region) and an SP active material in the IR and visible spectral regions. There is an increasing interest to investigate the metal electrolyte interface also in the near UV range to study e.g. such processes as water and organic absorption, respectively electrochemically modified surface topology and field induced modifications of the electron density at the surface.

However, in this spectral region, the excitation of SP's on Ag is not possible due to the onset of interband transitions at 3.8 eV — the effective Ag-plasma frequency. To solve this problem we have designed a thin film stratified electrode [6]. It consists of an optically thick Al-film as an SP-active metal up to the UV $\left(\hbar\omega_p \sim 15\ \text{eV}\right)$ covered by a thin Ag-coating (5-15 nm) to realize an electrochemically well defined contact to the electrolyte. We have applied this thin film electrode to study electrochemically induced surface roughness by the SP-technique [7].

The aim of the present paper is to study the optical properties of the Ag/Al samples by SP' excitation in air

(*) To whom correspondence should be adressed.

before they are used for electrochemical *in situ* measurements, described elsewhere [4].

We start the paper with the description of the experimental set-up which is developed to allow for experiments in the UV-range and to increase the sensitivity and precision.

The ATR experiments performed in a wide spectral range between 1.9 and 5 eV in Otto-geometry are reported in section 3. Around the effective plasma frequency of Ag (3.8 eV) the dispersion curve is characterized by a « back-bending » detected earlier by other authors [8, 9] in Kretschmann-geometry.

We describe this behaviour taking into account effects of spatial dispersion both in the Ag-film and in the Al-substrate. Our theoretical description outlined in section 4 is based on nonlocal optics proposed by Forstmann *et al.* [10, 11].

They used a hydrodynamic model of the conduction electron gas and additional boundary conditions for the metal/dielectric and metal/metal interfaces. It is shown (Sect. 5) that the influence of spatial dispersion cannot be neglected in our SP experiments even below the plasma frequency. An additional branch in the dispersion curve was detected in the region above the Ag-plasma frequency if the ATR-spectra were recorded by scanning the wavelength. Such modes have been predicted theoretically as coupled volume plasmon-surface plasmon modes but not detected up to now.

2. Description of the experimental arrangement.

The principle of the mounting is the excitation of SP's by ATR in focused light. A monochromatic lineary polarized beam is focused on the face of an hemicylindrical prism. In Otto-geometry used in the experiments described in this paper the sample is fixed at a distance of the order of the wavelength from the prism face. The excitation of a SP is characterized by a minimum in the p-polarized reflectivity $R_p(\varphi)$ as a function of the angle of incidence for fixed wavelength or $R_p(\lambda)$ as a function of the wavelength for a fixed angle of incidence.

With respect to the previous arrangement [13], the following modification has been brought in : a double beam system combined with a ratiometric lock-in technique ; a UV-transparent optics ; a circular step-motor drived rotation of a high sensitive broad band photomultiplier around the sample axis.

The experimental set-up is shown schematically in figure 1. Two sources were used : a xenon XB 0 150 (Osram) in the visible and a deuterium lamp D 200 F (Hanau) for the UV-range. The two spectra overlap in the near UV. The light is focused onto the entrance slit of a Czerny-Turner type monochromator H 25 (Jobin Yvon) which can be equipped by a visible or UV blazed grating.

By a system of two lenses and a pin hole a collimated spatially filtered monochromatic beam is formed. A

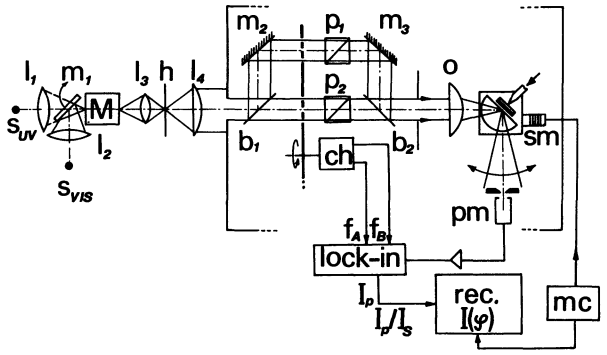

Fig. 1. — Experimental set-up. S_{uv}-deuterium lamp ; S_{vis}-xenon lamp ; l_1 and l_2 condensor lenses, l_3 and l_4-collimator lenses with pinhole h ; m_1, m_2, m_3 - mirrors ; b_1 and b_2-beam splitter foils ; p_1 and p_2 polarizers ; O-focalizing lens ; ch-chopper ; pm-photomultiplier ; sm-step motor ; mc-motor control unit.

diaphragm separates the central part (∅ 10 mm) of the beam which enters a beam splitting system. It is built by two very thin quartz foils (Fichou) coated for $R \sim T \sim 30$ % at 45° up to 200 nm (Achrovex coating, MTO) as beam splitters. The use of this very thin foil beam splitters avoids ghost patterns due to multiple reflections. The two beams passed a light chopper (Model 383 Ithaco). The blad has two series of holes (20 and 19) to form two signal slightly different in frequency. Two identical polarizers (Fichou) polarize each beam separately before they are resuperposed. A plan convex f 50 quartz lens (Fichou) focuses the beam at the exit face of the hemicylindrical ATR-quartz prism (R = 5 mm). Its axis is the rotation axis of a step motor drived arm carrying a head type broadband photomultiplyer (Hamamatsu R 761) with an adjustable entrance slit. The optical set-up has been adjusted by the help of a He-Ne Laser. All the optical devices are mounted on micropositioning units (Microcontrole). The step motor (0.001°/step) is controlled by a programmable unit (IT6 DCA, Microcontrole). It produces an analog signal proportional to the angular position of the photomultiplier which we have connected with an *x-y*-recorder.

The optical signals of beam A and B enter multiplexed the photodetector and are separated by a ratiometric lock-in system (Model 353, ITACO). The reference signals f_A and f_B are supplied by the chopper control unit. At the output we receive the amplified signals A and B or the normalized ratio A/B.

So it is possible to record directly the reflected intensities as a function of the angle of incidence. Figure 2 demonstrates a practical case. Beam A is parallel polarized (p), beam B perpendicular (s). The sample is an optically thick Ag-film on glass used in Otto arrangement. Signal A displays the SP-resonance minimum which is absent in B. Both signals are

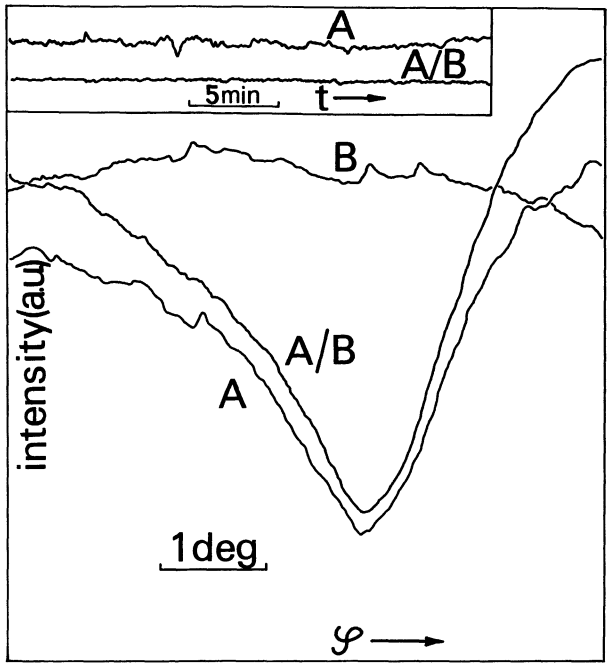

Fig. 2. — Recorded reflected intensities *vs* angle of incidence for an optical thick Ag-sample at $\lambda = 550$ nm. A-intensity of the p-polarized beam A ; B-intensity of the s-polarized beam B ; A/B-normalized reflectivity in ratiometric mode. Inset : intensity in simple lock-in (A) and ratiometric lock-in mode A/B *vs* time.

influenced by the beam geometry and source fluctuations (instabilities of the xenon arc). The normalized signal A/B has the advantage to be identical with R_p/R_s. Furthermore, the influence of source instabilities and beam inhomogenities are reduced. The inset of figure 2 shows the time stability of the normalized signal for fixed wavelength and angle of incidence.

The angular resolution of our experimental set-up is of about several minutes.

3. Experimental results.

Sample preparation and structural characterization have been outlined elsewhere [6]. Here we only summarize some major points. The Ag/Al samples are prepared by electron beam evaporation in ultrahigh vacuum ($p < 10^{-8}$ Torr) to avoid spontaneous oxidation of Al. The samples obtained are 5 nm thick Ag layers deposited onto 100 nm Al-films on polished quartz plates. The Ag overlayers are continuous van der Merve type grown as checked by TEM, SIMS and electrochemical stability tests. Thickness and growth rate are controlled by a calibrated quartz microbalance.

The optical experiment has been performed several hours after sample preparation. The optimum air gap between the sample and the prism face has been adjusted experimentally with the help of a micrometer screw so that the reflected p-polarizer light is minimal in the SP-resonance region. The adjustment is only in a certain spectral range at optimum. To cover a wide spectral range, we had to readjust the gap at other wavelength. The reflectivity was recorded between 1.9 and 5 eV. The angular position of the reflectivity minimum is indicative for the real part of the wavevector of the SP-excitation for a given wavelength. It is therefore just one point of the dispersion curve of the prism/air gap/Ag/Al-system. In figure 3 we have visualized the dispersion curve. The air gap was adjusted at 500 nm. The damping of the SP-resonance increases both in the red and in the blue ends of the spectrum. It is the misfit for the gap adjustment and the increasing damping of the Ag layer in the near UV which are responsible for this damping behaviour.

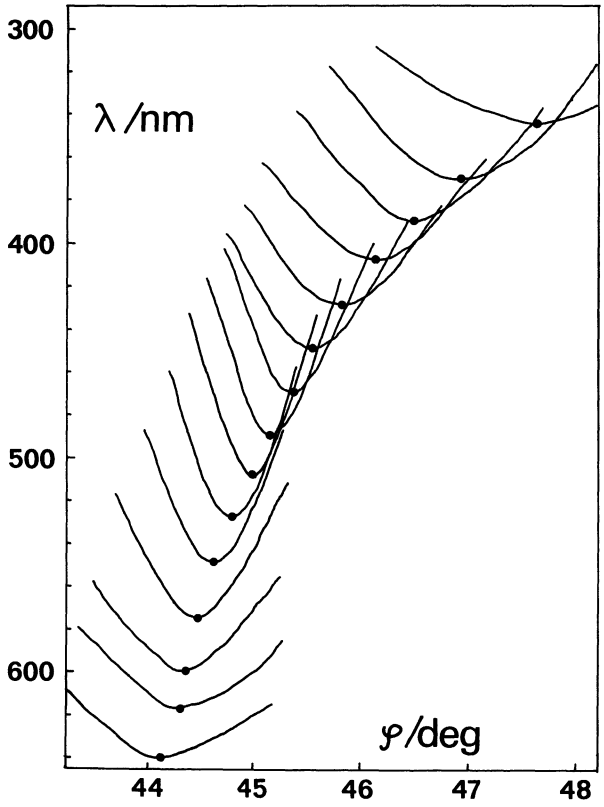

Fig. 3. — Recorded ATR spectra. The curves are shifted in the wavelength scale. Minimum position in λ corresponds to the wavelength for which the $R_p(\varphi)$ spectra are measured.

Figure 4 shows the dispersion for SP-excitation obtained in this manner at a Ag (5 nm)/Al (100 nm) quartz sample in Otto-geometry. The gap has been adjusted in four slightly overlapping regions : 1.9-2.75 eV, 2.54-3.1 eV, 2.92-3.54 eV (with xenon lamp) and $\hbar\omega > 3.3$ eV (deuterium lamp). The influence of the air-gap readjustment appears as small gaps in the dispersion curve which can be explained in the following way : the presence of a prism separated by the air-gap to the sample leads to a small shift of the dispersion curve of the free SP-excitation [14].

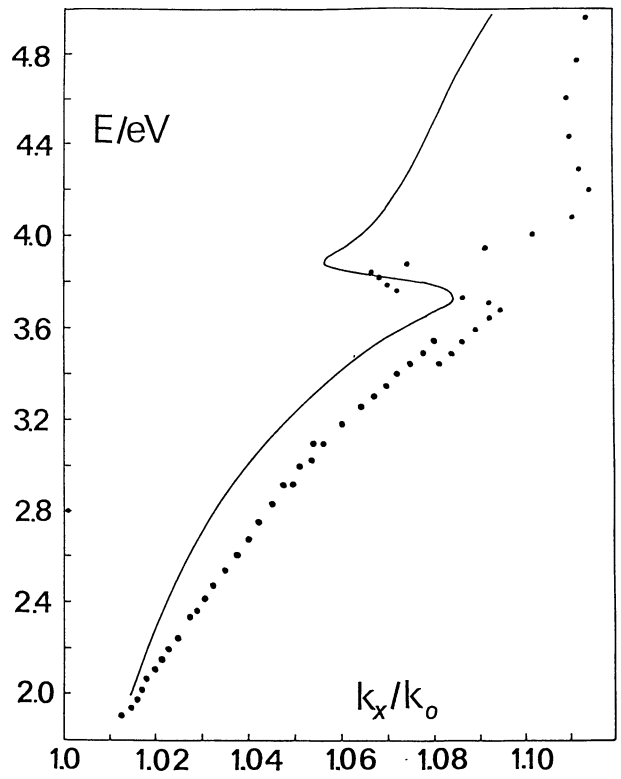

Fig. 4. — Dispersion of the surface plasmon excitation. Full circles — from ATR curves in angular scan. Continuous one — calculated dispersion curve of the free SP-excitation in nonlocal approach and increased damping (see text).

4. Theoretical model.

The dispersion curve in figure 4 shows a characteristic back bending around the 3.8 eV — the effective plasma frequency of Ag. This phenomena can be explained qualitatively in a simple way [15]: The thin Ag overlayer acts as a perturbation of the Al-SP-excitation by shifting and damping the resonance. The wavevector shift is positive for $\varepsilon_1\,\mathrm{Ag} < 0\,(\omega < \omega_p)$ and negative for $\varepsilon_1\,\mathrm{Ag} > 0\,(\omega > \omega_p)$ provided that $\varepsilon_{1_{Al}} < \varepsilon_{1_{Ag}} < 1$. The damping contributes to connect these two branches of the dispersion curve which leads to the observed structure. In the case of the energy scan for fixed angle of incidence, the two branches are separated by a gap.

For a detailed interpretation of the phenomena around the plasma frequency of silver, we have to take into account spatial dispersion. This includes the contribution of optically excited longitudinal plasma waves (PW) to the total optical response of the layered metal sample.

Lopez-Rios *et al.* [8] demonstrated the importance of spatial dispersion effects for the treatment of such Ag/Al samples if the thickness of the Ag overlayer is of the order of the wavelength of the PW.

In their calculations they have treated the Ag-film as spatially dispersive while the Al response has been assumed to be local in view of the high plasma frequency of Al (15 eV). Actually the Al substrate must also be treated nonlocally for the following reason: the matching conditions for the PW's at the Ag/Al interface must have an impact on the PW-propagation in the Ag layer even when the PW's in Al cannot propagate because of $\omega < \omega_p\,(\mathrm{Al})$.

The experimental results will be discussed in the framework of a hydrodynamic approximation for the electron gas both in the Al-layer and the Al-substrate. The formalism has been well described by several authors (see the review [18]) and will not be repeated here.

The total response of the metal will be regarded as a superposition of the contribution of the bound electrons *via* ε^b and the conduction electrons *via* the conductivity σ:

$$\varepsilon = \varepsilon^b - 4\,\pi i\sigma/\omega\,.$$

The core polarizability is treated locally $\varepsilon^b(\omega)$ while the conductivity is spatially dispersive $\sigma\,(w, k)$. The hydrodynamic approximation leads to a local transverse response:

$$\varepsilon^T(\omega) = \varepsilon^b(\omega) - \frac{\omega_p^2}{\omega\,(\omega + i\gamma)} \qquad (1)$$

and to nonlocal longitudinal one

$$\varepsilon^L(\omega, \mathbf{k}) = \varepsilon^b(\omega) - \frac{\omega_p^2}{\omega\,(\omega + i\gamma) - \beta k^2} \qquad (2)$$

with $\beta = \frac{3}{5}v_F^2$ and v_F being the Fermi velocity.

Our optical problem is characterized by three interfaces: prism/air gap, air gap/Ag, Ag/Al (Fig. 5) where the different fields have to be matched applying appropriate boundary conditions. At the prism/air interface there are only transverse fields. Two classical boundary conditions are sufficient: the continuity of the tangential components of the electric $E_t\,(\mathrm{I})$ and magnetic $H_t\,(\mathrm{II})$ fields.

At the air/Ag interface a third boundary condition is necessary to take into account the longitudinal field at the metal side. We use the well established additional

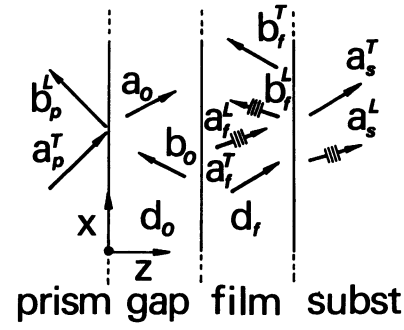

Fig. 5. — Model of considered ATR experiment. $a^{T,L}$, $b^{T,L}$ amplitudes of the transverse (T) electromagnetic and longitudinal (L) plasma waves in the prisme (p), the air-gap (o), the Ag-film (f) and the Al-substrate (s).

boundary condition proposed by Sauter [16] : the continuity of the normal component of the current density. By combination with the boundary condition for the displacement vector, Sauter's condition can be expressed as the continuity of

$$\varepsilon^{b} E_{n} . \qquad \text{(III)}$$

At the intermetallic interface there are a transverse and a longitudinal fields at both sides of the interface. To determine all the four amplitudes we shall use a fourth boundary condition proposed by Forstman *et al.* [10] : the continuity of the normal component of the energy current density. We note it in the practical form suggested in [20] :

$$\frac{1}{\nu} E_{t}^{L} \qquad \text{(IV)}$$

with $\nu = \varepsilon^{b}/\varepsilon^{T} - 1$ and E_{t}^{L} being the tangential component of the longitudinal field.

For the notation of the fields we refer to figure 5. The transverse fields in medium « i » are

$$\mathbf{E}_{i}^{T} = a_{i}^{T}\left(\mathbf{Y}_{0} \wedge \mathbf{K}_{i}^{T}\right) e^{i\left(\frac{\omega}{c}\mathbf{K}_{i}^{T}\mathbf{r} - \omega t\right)} + b_{i}^{T}\left(\mathbf{Y}_{0} \wedge \mathbf{K}_{i}^{T'}\right) e^{i\left(\frac{\omega}{c}\mathbf{K}_{i}^{T'}\mathbf{r} - \omega t\right)} \qquad (3)$$

$$\mathbf{H}_{i}^{T} = a_{i}^{T}\,\varepsilon_{i}^{T}\,\mathbf{Y}_{0}\, e^{i\left(\frac{\omega}{c}\mathbf{K}_{i}^{T}\mathbf{r} - \omega t\right)} + b_{i}^{T}\,\varepsilon_{i}^{T}\,\mathbf{Y}_{0}\, e^{i\left(\frac{\omega}{c}\mathbf{K}_{i}^{T'}\mathbf{r} - \omega t\right)} \qquad (4)$$

and the longitudinal fields are

$$\mathbf{E}_{i}^{L} = a_{i}^{L}\mathbf{K}_{i}^{L} e^{i\left(\frac{\omega}{c}\mathbf{K}_{i}^{L}\mathbf{r} - \omega t\right)} + b_{i}^{L}\mathbf{K}_{i}^{L'} e^{i\left(\frac{\omega}{c}\mathbf{K}_{i}^{L'}\mathbf{r} - \omega t\right)} \qquad (5)$$

with i = p (prism), o (gap), f (Ag-film), s (Al-substrate), and Y_0 being the unit vectors of the reference system. There are no magnetic fields associated to the PW's since curl $E = 0$. In the dielectric media there are no longitudinal fields hence $a_{p,0}^{L} = b_{p,0}^{L} = 0$.

The wavevectors of transverse fields are obtained *via* the dispersion relation for electromagnetic waves

$$\left(K_{i}^{T}\right)^{2} = \varepsilon_{i}^{T}(\omega) \qquad (6)$$

and those of the longitudinal fields via the implicit dispersion relation of PW's $\varepsilon_{i}^{L}\left(\omega, \mathbf{K}_{i}^{L}\right) = 0$ which yields [18]

$$\left(K_{i}^{L}\right)^{2} = \frac{c^{2}}{\omega^{2}\beta_{i}}\left[\omega\left(\omega + i\gamma_{i}\right) - \frac{\omega_{pi}^{2}}{\varepsilon_{i}^{b}(\omega)}\right]. \qquad (7)$$

Application of boundary conditions I-IV and use of Snell's law ($K_{ix} = K_{x} = \sqrt{\varepsilon_{p}}\sin$ and $K_{iz}' = -K_{iz}$) leads to an inhomogeneous system of 9 equations for the 9 unknown field amplitudes as function of the incoming field amplitude. (We have set the amplitude of the incoming transverse wave $a_{p} = 1$.)

$$\begin{bmatrix}
-K_{pz}^{T} & -K_{0z}^{T} & K_{0z}^{T}\alpha_{0}^{T} & 0 & 0 & 0 & 0 & 0 & 0 \\
\varepsilon_{p}^{T} & -\varepsilon_{0}^{T} & -\varepsilon_{0}^{T}\alpha_{0}^{T} & 0 & 0 & 0 & 0 & 0 & 0 \\
0 & K_{0z}^{T}\alpha_{0}^{T} & -K_{0z}^{T} & -K_{fz}^{T} & K_{fz}^{T}\alpha_{f}^{T} & -K_{x} & -K_{x}\alpha_{f}^{L} & 0 & 0 \\
0 & \varepsilon_{0}^{T}\alpha_{0}^{T} & \varepsilon_{0}^{T} & -\varepsilon_{f}^{T} & -\varepsilon_{f}^{T}\alpha_{f}^{T} & 0 & 0 & 0 & 0 \\
0 & \varepsilon_{0}^{T}K_{x}\alpha_{0}^{T} & \varepsilon_{0}^{T}K_{x} & -\varepsilon_{f}^{b}K_{x} & -\varepsilon_{f}^{b}K_{x}\alpha_{f}^{T} & \varepsilon_{f}^{b}K_{fz}^{L} & -\varepsilon_{f}^{b}K_{fz}^{L}\alpha_{f}^{L} & 0 & 0 \\
0 & 0 & 0 & K_{fz}^{T}\alpha_{f}^{T} & -K_{fz}^{T} & K_{x}\alpha_{f}^{L} & K_{x} & -K_{x}^{T} & -K_{x} \\
0 & 0 & 0 & \varepsilon_{f}^{T}\alpha_{f}^{T} & \varepsilon_{f}^{T} & 0 & 0 & -\varepsilon_{s}^{T} & 0 \\
0 & 0 & 0 & \varepsilon_{f}^{b}K_{x}\alpha_{f}^{T} & \varepsilon_{f}^{b}K_{x} & -\varepsilon_{f}^{b}K_{fz}^{L}\alpha_{f}^{L} & \varepsilon_{f}^{b}K_{fz}^{L} & -K_{x}\varepsilon_{s}^{b} & K_{s}^{L}\varepsilon_{s}^{b} \\
0 & 0 & 0 & 0 & 0 & \frac{K_{x}}{\gamma_{f}}\alpha_{f}^{L} & \frac{K_{x}}{\gamma_{f}} & 0 & \frac{K_{x}}{\gamma_{s}}
\end{bmatrix}
\times
\begin{bmatrix} b_{p}^{T} \\ a_{0}^{T} \\ b_{0}^{T} \\ a_{f}^{T} \\ b_{f}^{T} \\ a_{f}^{L} \\ b_{f}^{L} \\ a_{s}^{T} \\ a_{s}^{L} \end{bmatrix}
=
\begin{bmatrix} -K_{pz}^{T} \\ -\varepsilon_{p} \\ 0 \\ 0 \\ 0 \\ 0 \\ 0 \\ 0 \\ 0 \end{bmatrix} \qquad (8)$$

with $\alpha_{i}^{T,L} = \exp(ik_{iz}^{T,L} d_{i}) \quad i = 0, f.$

From this system we can get informations to interprete our experiments :

(i) The homogeneous 7 × 7 subsystem in the dashed brackets describes the fields of the free Ag/Al system in contact with air. Since there are no incident fields a nonvanishing outcoming amplitude b_{0}^{T} corresponds to a surface plasmon excitation. These eigensolutions are found by setting the determinant of the corresponding 7 × 7 coefficient matrix equal to zero. For given real frequency we obtained numerically the complex wavevector component $K_{x} = K_{x1} + iK_{x2}$. This 7 × 7 matrix is formally equivalent to the matrix given by Forstmann *et al.* [11] to describe a spatially dispersive stepped surface of Al.

(ii) From the whole nonhomogeneous 9×9 equations system the reflectivity of the ATR experiment can be calculated. It has been solved for the amplitude of the reflected transverse field in the prism $\left(b_p^T\right)$ by application of Kramers rule for given real frequency and angle of incidence. Then one has $R_p(\omega, \varphi) = \left|b_p^T\right|^2$. The angular position of the resonance minimum is related to K_{x1} of the dispersion relation while its broadness accounts for the damping parameter K_{x2}.

Differences can arise in the wavevectors obtained in (i) and (ii). While the approach (i) gives all possible eigensolutions (ii) describe the actually excited ones in an ATR experiment including the prism and air gap influence on the field distribution.

For nummerical application to Ag the Johnson/Christie parameters [19] were used. Since they have been measured in reflection-transmission experiments in quasinormal incidence where PW's cannot be excited it is justified to use these values as $\varepsilon_f^T(\omega)$.

The parameters used in the free electron part $\left(\omega_p, \gamma\right)$ are derived from measurements in the infrared region far from interband transitions. We used the same parameters as in [27] : $\hbar\omega_p = 9$ eV and $\gamma = 2.62 \times 10^{13}\ s^{-1}$.

The bound electron contribution ε^b of Ag has been obtained by subtracting the free electron part from the experimentally determined dielectric constant [19].

For the nonlocality parameter β_{Ag} we used the value $2.57 \times 10^{12}\ m^2/s^2$ obtained experimentally by fitting the dispersion curve of PW's in the optical region [17]. It is 2.2 times larger than the value calculated with one s-electron per atom. This has been explained in [17] by the contribution of the d-electrons in the spectral region where interband transitions occur.

For Al a quasi free electron behaviour can be assumed in the frequency regions we are interested in ($\lambda < 800$ nm where weak interband transitions occur). Hence $\varepsilon_{Al}^b = 1$. For the Drude parameters we have used

$$\hbar\omega_p = 14.88\ \text{eV}, \quad \gamma = 9.1 \times 10^{14}\ s^{-1}\ [9].$$

The nonlocality parameter for Al can be calculated directly from the free electron concentration in Al (3 electrons per atom) which leads to $\beta_{Al} = 2.7 \times 10^{12}/s^2$.

5. Discussion.

Let us first discuss the dispersion curves obtained by scanning the k-vector for fixed wavelength. The corresponding implicit dispersion relation must be solved for real energy and complex wavevector components.

In figure 6a, we have drawn the calculated dispersion curves for three cases in the vicinity of the Ag-plasma frequency where nonlocal effects are expected to be important : a) local treatment, b) local substrate and nonlocal film, c) nonlocal film and nonlocal substrate.

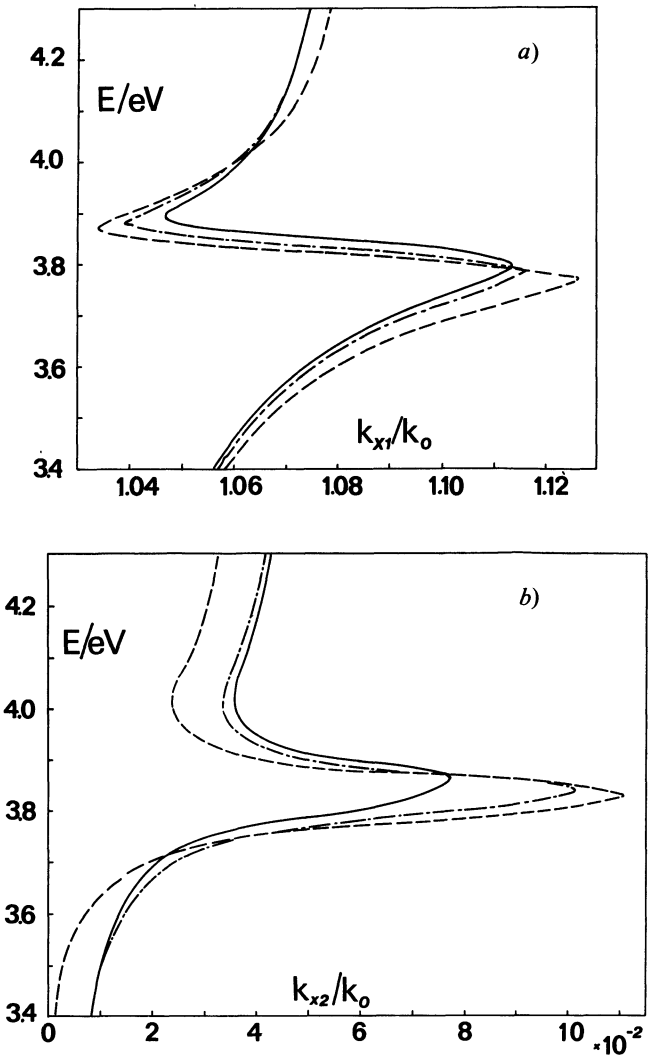

Fig. 6. — Calculated dispersion curves for a Ag(5 nm)-/Al-sample in the local case (dashed) ; nonlocal film and local substrate (dashed-dotted) ; completely nonlocal treatment (continuous line). a : energy *vs.* real part of k_x/k_0 ; b : energy *vs.* imaginary part of k_x/k_0.

For an evaluation of the importance of nonlocal effects, we estimate the difference $(\Delta\varphi)$ of the angular positions of the SP resonance in the local and nonlocal treatment from figure 6.

For $\hbar\omega = 3$ eV $\Delta\varphi$ is only of about several minutes, but for $\hbar\omega = 3.5$ eV, we get $\Delta\varphi \sim 0.2°$ and the difference in the backbending amplitude is of about 1.3°. The experimental angular resolution is of about several minutes. So far we conclude that PW's have to be included in the interpretation of the experiments.

The influence of PW's seems to be most important in the spectral region where the backbending becomes smaller and in this way closer to experiment (Fig. 4), if spatial dispersion is taken into account both in the film and in the substrate.

In a completely local treatment the backbending reflects a singularity of the SP-dispersion due to the plasma behaviour of the film ($R_e\ \varepsilon_{Ag}(\omega_p) = 0$). This is evident if we look at the approximative formula for the wavevector shift ΔK_f caused by a very thin film $(d_f < \lambda)$ on the SP-dispersion [14]

$$\Delta K_f = K_s \frac{\varepsilon_0\ \varepsilon_s}{(\varepsilon_0 - \varepsilon_s)\left[-(\varepsilon_0 + \varepsilon_s)\right]^{3/2}} \times \times \left[\varepsilon_0 + \varepsilon_s - \frac{\varepsilon_0\ \varepsilon_s}{\varepsilon_f} - \varepsilon_f\right] 2\ \pi d_f/\lambda \quad (9)$$

with $K_s = \left[\varepsilon_0\ \varepsilon_s/(\varepsilon_0 + \varepsilon_s)\right]^{1/2}$ being the wavevector of the SP of the unperturbed metallic substrate ε_s in contact with ε_0.

A nonlocal treatment allows for the excitation of longitudinal PW's. So the system gets additional degrees of freedom to cancel the singularity in the local case. This is the same behaviour as noticed by Kempa *et al.* [20] in the nonlocal treatment of the ellipsometric experiments of metallic films on metals.

This can be illustrated by looking for the damping behaviour $\mathrm{Im}(K_x)$ drawn in figure 6b. We notice a decrease of the plasma peak around ω_{pAg} for the nonlocal approach compared with the local one. Outside the peak, the damping is greater in the spatially dispersive case : part of the SP energy is dissipated into the volume-PW's.

Comparing the curves in figure 6 corresponding to a local or nonlocal treatment of the Al-substrate another important feature is observed : a nonlocal treatment of both the film and the metallic substrate is necessary even in the case when PW's cannot propagate in the Al-substrate due to $\omega < \omega_{pAl}$.

The local treatment of the substrate as used in [9] has an impact on the PW propagation in the Ag-layer *via* the matching conditions at the Ag/Al-interface.

Nevertheless, the backbending remains too large even in the nonlocal case if the Johnson/Christie damping parameter is used. In the right side of figure 7, the dispersion curves calculated with a Drude damping parameter increased by a factor ten are drawn. Even in this case, the influence of the spatial dispersion remains to be a noticeable effect. The value which gives the best fit to the experimental behaviour is $\hbar\gamma = 0.24$ eV. We can explain this phenomena by the impact of surface scattering on the lifetime of the electrons in this very thin polycrystalline Ag-layer [21].

In figure 4, the dispersion curve for this case is also drawn. With respect to the experimental data, there is a shift in the k-scale which increases with the energy. We attribute this effect both to the influence of the prism which is not considered in the calculation of the dispersion curve and to surface roughness. Microscopic surface roughness can be described phenomenologically

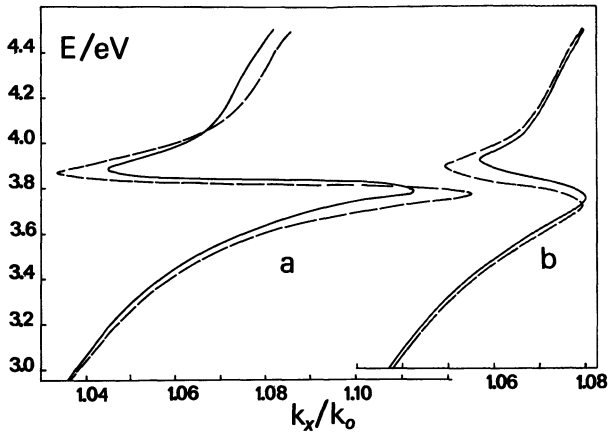

Fig. 7. — Calculated influence of the damping in the Ag-film on the SP-dispersion for a Ag-(5 nm)/Al-sample in the local (dashed) and nonlocal treatment (continuous) a) damping parameter according to [19] ; b) damping parameter increased by factor 10.

by an effective absorbing overlayer [22] leading to a shift of the dispersion curve. This effect should increase with photon energy as observed in our experiments.

We shall now turn our attention to the behaviour of the system at high energy and discuss specially the ATR spectra recorded in energy scan for fixed angle of incidence around the Ag-plasma frequency (between 3.1 and 5 eV). The R_p/R_s curves shown figure 8 display two minima : a very pronounced one around 3.8 eV and a second very flat one. We have presented figure 9 the corresponding dispersion curve measured by scanning the angle of incidence at fixed photon energy, in the same energy range.

In chapter 4 we have explained that the SP-dispersion curve of the system under consideration consists of two separated branches if it has been measured in *E*-scan, one below and one above the plasma frequency of the film. However, in this experiment (Fig. 8), the lower branch is not excited. The reason is that the air gap has been adjusted to allow for SP-excitation for energies $E > \hbar\omega_{pAg}$. It is too small for an efficient coupling to the SP's of the lower branch.

We have calculated the reflectivity curves *vs* energy for different angles of incidence between 3 and 5 eV using equation (8). It is found that the lower branch disappears for gap width smaller than 150 nm. Figure 10 shows the calculated reflectivity curves for a fixed gap (125 nm) in the local and nonlocal treatment (nonlocality of both the film and the substrate). This gap has been chosen to give an optimum fit to the experimental reflectivity curves.

Comparing with the experimental curves we conclude :

1. Nonlocal effects become more important for increasing angle of incidence and hence greater wavevector.

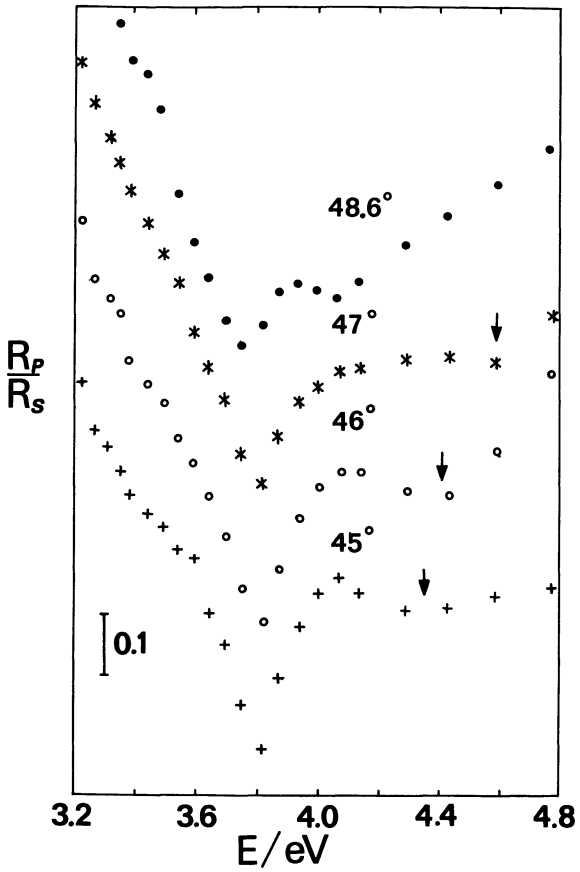

Fig. 8. — ATR spectra in energy scan for fixed angles of incidence for a Ag-(5 nm)-Al-sample Experimental results at fixed air gap

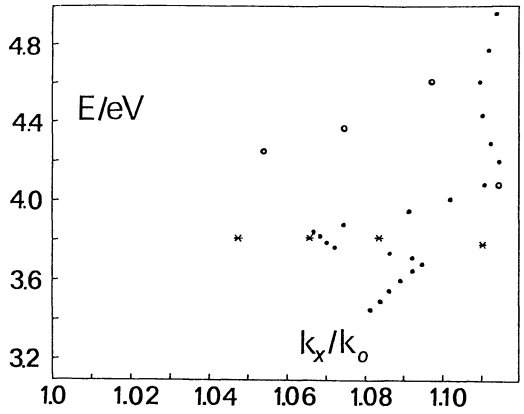

Fig. 9. — Dispersion of the surface plasmon excitation at high photon energy, full circles. From ATR curves in angular scan. Cross and open circles. From ATR curves in energy scan.

2. The general shape of the experimental curves is well reproduced, namely the main minimum around 3.8 eV. This minimum is nearly fixed at ω_{pAg} up to a certain angle.

3. For greater angles there is a splitting of the resonance : a sharp one, about 50 meV below ω_{pAg}, and a second flatter one at $\hbar\omega = 4.1$ eV (Fig. 8, φ = 48.6°). The same behaviour is obtained only in the nonlocal approach (Fig. 10, 49°). The localy calculated curve displays an additional structure between the two minima which have not been observed experimentally. Furthermore, the amount of the negative shift of the principal minimum is better reproduced in the nonlocal treatment.

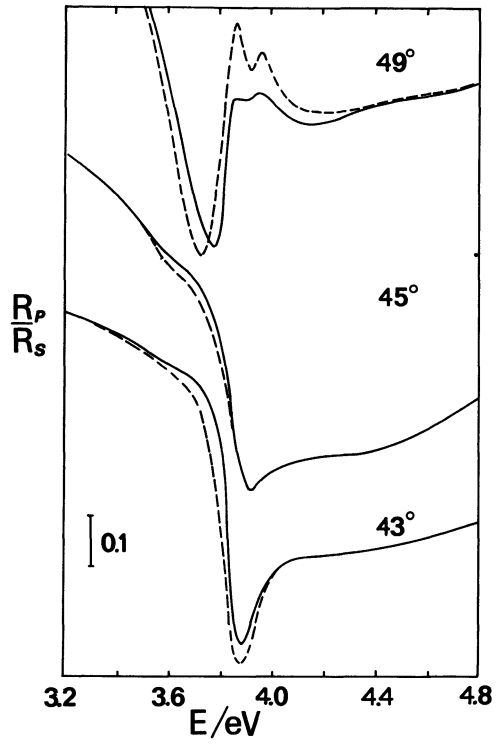

Fig. 10. — Calculated ATR in energy scan for fixed angle of incidence and fixed air gap (125 nm). Continuous line : non local approach ; dashed line : local calculations.

4. There is a small difference (+ 50 meV) in the absolute energy position of the principal minimum with respect to the experimental behaviour. The same is valid for the SP-dispersion curve measured in *k*-scan (Figs. 4, 6). We attribute this fact to the choice of the Johnson/Christie parameters for the description of our Ag-film. Nearly the same difference (~ 70 meV) in the position has been observed in [17] for electrodeposited thin Ag-layers.

5. There is additional very flat minima in the energy region above ω_{pAg} (Fig. 8 arrows) which are not reproduced within our model calculations. (We have tried a variety of air gaps). The energy position of these minima marked in figure 9 between 4.2 and 4.6 eV seems to reflect an additional branch of the dispersion curve. It is probably not a pecularity of the Ag-dielectric function because of the k-dependence of the minima position.

We attribute these minima to higher coupled SP-volume plasmon modes predicted theoretically by diffe-

rent authors [23, 24, 11] but not detected experimentally up to now.

Equiluz and Quinn [23] calculated the Sp-dispersion within a hydrodynamic model in the electrostatic limit taking into account a « smooth » electron density profile at the metal surface. They found additional branches in the SP-dispersion which disappear for a sharp surface profile. The authors pointed out that these modes (at least the lowest dipole type one) should be detectable in ATR measurements carried out in energy scan to avoid backbending effects — exactly the kind of experiments we have done.

One could imagine these modes as standing plasma wave modes in a thin film [24]. But we can exclude that the whole Ag-film of 50 Å is the supporting medium for these standing waves : otherwise our nonlocal calculation should exhibit this effect. The calculation shows that the absorption in this energy region is too high to allow for an interference of plasma waves over the whole film thickness of 50 Å. In this context, we do not agree with the results published recently by Pimpale *et al.* [25] for the energy position of standing plasma waves in Ag-films. The authors used a free electron model in the energy region above 3.8 eV where the interband transition cannot be neglected by any assumption. This affects also the actual form of the additional boundary conditions.

We conclude that a smooth electron density profile both at the Ag-Vacuum and the Ag/Al-interface [26] could be responsible for the detected effect. An additional argument for this conclusion is the following one. The position of the first minimum is exactly fixed at 3.8 eV (Fig. 8 $\varphi = 45°, 46°, 47°$) before the splitting at 48.6° occurs. Calculated spectra exhibit a slow increase of its energy position even in the nonlocal approach in the framework of our model. The assumption of a smooth electron density profile leads to a plateau in the regular SP-dispersion branch for small wavevectors i.e. in the optical region [11], [23] as observed (Fig. 9).

To involve these considerations it is necessary to refine our model to consider the electron density decay at the metal/vacuum and the intermetallic interface which will be done in a further publication. To avoid too large matrices (each intermetallic interface will add 4 equations) we have developed a flexible multilayer method involving spatial dispersion in the framework of the hydrodynamic approximation [28].

Acknowledgments.

We would like to thank the Centre National de la Recherche Scientifique for financial support granted to M. Abraham during 1983/84. We thank J.P. Rolland (C.N.R.S.-Meudon) for his technical support and G. Vuye (Université Paris VI) for suggesting the design of the beam splitters. We are greateful to Prof. Forstmann (FU-Berlin-West) and U. Trutschel (TH-Ilmeneau) for stimulating discussions and Prof. G. Paasch (TH-Ilmeneau) for the critical reading of the manuscript.

References

[1] AGRANOVITCH, W. M., MILLS, D. L. (Edt's), *Surface Polaritons. Electromagnetic waves at surfaces and interfaces* (Nauka, Moscou) 1985.
[2] ABELES, F., LOPEZ-RIOS, T. and TADJEDDINE, A., *Sol. State Commun.* **16** (1975) 843.
[3] KOLB, D. M., in [1] p. 207.
[4] TADJEDDINE, A., ABRAHAM, M. and HADJADJ, A., *J. Electroanal. Chem.* (1986) 869.
[5] KRETSCHMANN, E., *Opt. Commun.* **26** (1978) 41.
[6] ABRAHAM, M., ROLLAND, J. P., SCHIFFMACHER, G., TADJEDDINE, A., *Surf. Sci.* **146** (1984) 351.
[7] TADJEDDINE, A., ABRAHAM, M., *Phys. Rev.* **B 32** (1985) 5496.
[8] LOPEZ-RIOS, T., ABELES, F., VUYE, G., *J. Physique* **39** (1985) 645.
[9] LOPEZ-RIOS, T., ABELES, F., VUYE, G., *J. Physique Lett.* **40** (1979) L-343.
[10] FORSTMANN, F., STENSCHKE, J., *Phys. Rev. Lett.* **38** (1977) 1365.
[11] FORSTMANN, F., STENSCHKE, H., *Phys. Rev. B* **17** (1978) 1489.
[12] OTTO, A., *Z. Phys.* **216** (1968) 398.
[13] TADJEDDINE, A., CHIALI, S., COSTA, M., *J. Chim. Phys.* **80** (1983) 785.
[14] ABELES, F., *J. Physique Colloq.* **38** (1977) C5-67.
[15] LOPEZ-RIOS, T., *Opt. Commun.* **17** (1976) 342.
[16] SAUTER, F., *Z. Physik* **203** (1967) 488.
[17] PIAZZA, G., KOLB, D. M., KEMPA, K., FORSTMANN, F., *Sol. State Commun.* **51** (1984) 905.
[18] FORSTMANN, F., GERHARDTS, R. R., in *Festkörperprobleme* Adv. in Solid State Physics, vol. 21 Ed. Treusch (Vieweg, Braunschweig) 1982.
[19] JOHNSON, P. B., CHRISTIE, R. W., *Phys. Rev.* **B 6** (1972) 4370.
[20] KEMPA, K., GERHARDTS, R. R., *Surf. Sci.* **150** (1985) 157.
[21] FUCHS, K., *Proc. Camb. Philos. Soc.* **34** (1983) 100.
[22] ASPNES, D. E., *Thin Solid Films* **89** (1982) 249.
[23] EQUILUZ, A., QUINN, J. J., *Phys. Rev.* **B 14** (1976) 1347.
[24] LOPEZ-RIOS, T., *Sol. State Commun.* **37** (1981) 765.
[25] PIMPALE, A., PARANJAPE, B. V., *Surf. Sci.* **161** (1985) 69.
[26] FERRANTE, J., SMITH, J. R., *Phys. Rev.* **B 31** (1985) 3427.
[27] KOETZ, R., KOLB, D. M., FORSTMANN, F., *Surf. Sci.* **91** (1980) 489.
[28] ABRAHAM, M., TRUTSCHEL, U., TADJEDDINE, A., *Opt. Commun.* **58** (1986) 369.